A CMOS Microarray with On-Chip Decoder /Amplifier and Its Integration with a Bio-Nano-System*

Zhang Lei[1,†], Gu Zhen[2], Yu Zhiping[1], He Xiangqing[1], and Chen Yong[2]

(1 *Institute of Microelectronics, Tsinghua University, Beijing* 100084, *China*)
(2 *Department of Mechanical and Aerospace Engineering, California NanoSystems Institute, University of California, Los Angeles, CA* 90095, *USA*)

Abstract: A fully integrated CMOS bio-chip is designed in a SMIC 0.18μm CMOS mixed signal process and successfully integrated with a novel bio-nano-system. The proposed circuit integrates an array of 4×4 (16 pixels) of 19μm×19μm electrodes, a counter electrode, a current mode preamplifier circuit (CMPA), a digital decoding circuit, and control logics on a single chip. It provides a −1.6∼1.6V range of assembly voltage, 8bit potential resolution, and a current gain of 39.8dB with supply voltage of 1.8V. The offset and noise are smaller than 5.9nA and 25.3pArms, respectively. Experimental results from on-chip selective assembly of 30nm poly (ethylene glycol) (PEG) coated magnetic nano-particles (MNPs) targeted at biosensor applications are included and discussed to verify the feasibility of the proposed circuits.

Key words: CMOS bio-chip; CMOS integrated microarray; fully integration; current mode preamplifier; selective assembly; magnetic nano-particles
EEACC: 1205; 1280; 3120
CLC number: TN432 **Document code**: A **Article ID**: 0253-4177(2008)10-1947-09

1 Introduction

Biomedical technology has emerged as one of the most promising developments in the 21st century together with nanoelectronics industries. Recently, DNA molecule based biosensors have been extensively reported in the literature[1∼3]. However, limited by the sensor material and fabrication process, biosensors currently being used are mostly implemented in a discrete way. But in real applications (e.g., examining DNA and proteins in a blood sample), hundreds of independent biosensors in the micrometer scale with drivers and readout circuits are required, which is prohibitive to realize if implemented in discretely. Naturally, the CMOS integrated bio-system (IBS) which monolithically integrates the biomedical electrode arrays and ASICs in a single chip is avidly expected. Some CMOS integrated microarray (IMA) circuits have been implemented in standard CMOS processes. Xu *et al*. incorporated the sliver-enhanced optical protocol and measured the optical current in each activated site by CMOS readout circuits[4]. However, without signal pre-amplificaiton stage, it relies on accurate low current measurement to ensure the sensitivity, thus requiring large device area and expensive instruments. Han, Augustyniak, and Thewes used in-pixel double-integrator circuits, amplifiers, or AD converters to achieve the expected resolutions[5∼7]. But this introduced the complexities of pixel circuits and prevents the further down scaling of site area in the future. Furthermore, these works rely on a conventional gold—sulphur (Au—S) bond to self-assemble a DNA monolayer on the electrode surface and detect the complementary DNA molecules in the electrolyte. However, the non-specific Au—S bond can not selectively assemble the DNA monolayer on the targeted electrode, limiting the specificity and diversity of the following sensing procedure. Although efforts have been made for the patterning of DNA assembly by introducing an electric releasing scheme, this scheme is complicated for electric controlling and processing, and is also time consuming (typically over 10 hours).

In this paper, an IMA circuit with a pixel decoder, driver, shared current mode preamplifier (CMPA), and control logics, is integrated with a bio-nano-system. We use a novel electromagnetically assisted assembly scheme for the first time, and it is designed in a SMIC 0.18μm CMOS mixed signal process. In this circuit, the electrode array integrates the 16 pixels of 19μm×19μm working electrodes and a 140μm×19μm counter electrode on a single chip. Compared to the conventional discrete biosensors and the reported works, the proposed IMA has many advantages as

* Project supported by the National Natural Science Foundation of China (Nos. 60236020, 90307016), the Intel Foundation, the University Program of SMIC, and the Private Research Grant Provided by Dr. Dan Yang in CA, USA
† Corresponding author. Email: zl99@mails.tsinghua.edu.cn
Received 6 April 2008, revised manuscript received 3 June 2008

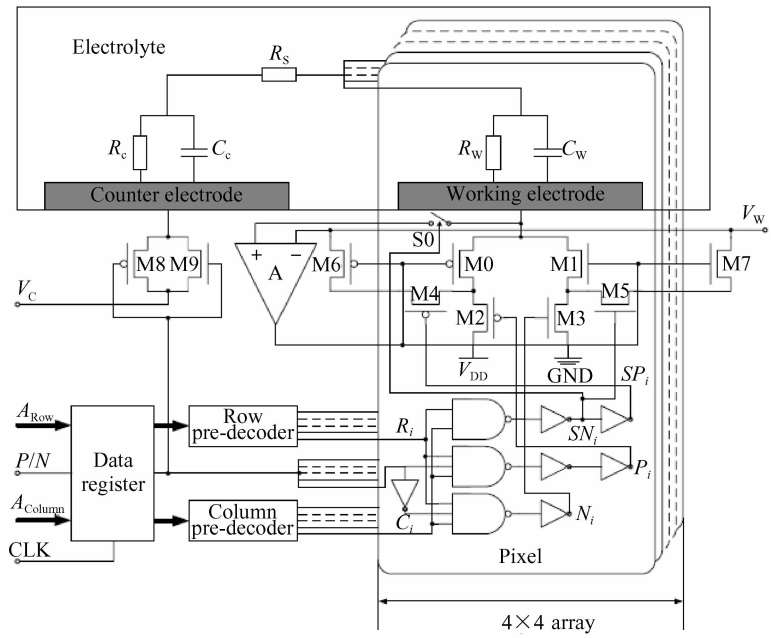

Fig. 1 System schematics of proposed CMOS IMA circuit

follows. (1) It integrates a bio-medical electrode array with main-stream CMOS technology, which substantially reduces the cost and complexity of fabrication and electric interconnection, and saves chip area as well; (2) It introduces the two stage decoding scheme (pre-decoding and pixel decoding) to selectively activate one of the pixels, which makes the circuit regular in architecture and easy to lay out; (3) It eliminates the complex in-pixel double-integrator, amplifiers, or AD converters, but uses an out-pixel CMPA shared by all pixels to amplify the current from the activated pixel before it goes to the following processing stages, e. g., AD, integrator, DSP, etc, which simplifies the pixel circuitry and thus further shrinks the pixel area; (4) It uses the novel electromagnetically assisted assembly scheme, based on charged magnetic nano-particles (MNPs), to simplify the assembly process and enhance the specificity and efficiency (the assembly time is only 60s) as well; (5) It uses aluminium (Al) as the electrode material, which is completely compatible with CMOS technology and straightforward to fabricate. The proposed circuit is further verified by experiments from the on-chip selective assembly of the prototype of 30nm negatively charged poly (ethylene glycol) (PEG) coated MNPs in the aqueous buffer onto an address-activated working electrode by applying a positive assembly voltage with respect to the counter electrode. Moreover, since the PEG coated MNPs are capable of conjugating with multiple types of DNA molecules, proteins, and antibodies[8,9], it provides a novel platform for bio-sensing applications and is believed to be a promising candidate for improving the bio-sensing efficiency, specificity, and diversity of IBS.

2 Circuit design and analysis

The system topology of the proposed CMOS IMA circuit is illustrated in Fig. 1. It is designed with an array of 16 pixels and a $140\mu m \times 19\mu m$ counter electrode. Each of the pixels is a $19\mu m \times 19\mu m$ electrode. A two-stage address decoding approach (predecoding and pixel decoding) is introduced to selectively activate the working electrodes of the IMA. An on-chip CMPA circuit is implemented to control the working electrode potential. It also receives and amplifies the pixel current using the negative feedback mechanism and the input regulated current mirror.

2.1 Electrode decoding logic

On the rising edge of the clock CLK, logic states of A_{Row}, P/N, and A_{Column} are locked into the data register and propagated to the decoding stage. The decoding mechanism is realized by the two-stage decoding logic composed of row-column pre-decoder and pixel decoder. The standard transformation from input binary code to $1/N$ code is performed by the pre-decoder circuit, with the output of logic signals R_i and C_i for an arbitrary pixel i, where $i = 1, 2, \cdots, 16$, as shown in Fig. 1.

In the pixel decoder, if and only if both R_i and C_i are activated (logic "11"), S0, M4, and M5 are switched on by logic signals SP_i and SN_i, the ith working electrode is connected to a positive voltage of $V_W - V_C$ (or a negative voltage of $-|V_W - V_C|$) by the pixel logic gates, pMOS transistors M0, M2, and

Table 1　Truth table of the pixel decoding logic

R_i	C_i	P/N	P_i	N_i	SP_i	SN_i
0	×	×	1	0	1	0
×	0	×	1	0	1	0
1	1	0	1	1	0	1
1	1	1	0	0	0	1

M4 (or nMOS transistors M1, M3, and M5), depending on the logic "1" or "0" of the state signal P/N, where P_i and N_i are pixel logic signals controlling transistors M2 and M3. Meanwhile, all the other combinations of R_i and C_i (logic "00", "01", and "10") will close S0 and transistors M2～M5, and thus float the working electrode to the high resistance state with only ～10pA of leakage current to the electrolyte. The truth table of the proposed pixel decoding architecture is illustrated in Table 1.

2.2　Current mode preamplifier (CMPA)

Quantitative analysis of a bio-nano-system requires the measurement of currents within the electrolyte. But since these currents are mostly on the order of nano or sub-nano amperes, direct measurement is sensitive to off-chip fluctuations and noises. Therefore, pre-amplification of the current in the on-chip low noise environment is preferable.

The CMPA circuit to stabilize the working electrode potential and amplify the bio-assembly current[10,11] is the major part of the proposed IMA since it confines the potential resolution and noise current. Preliminary experiments of the electromagnetically assisted assembly of MNPs in the aqueous buffer have been made on the customized working electrode (without integration with the CMOS circuit), and the specifications are summarized in Table 2.

To meet the specifications in Table 2, in the CMPA, the current amplification based on the complimentary architecture of input-regulated current-mirror is introduced in the design to provide the capability of bidirectional assembly and nano-ampere current amplification (based on our previous works in Refs. [10] and [11]), where the N and P branches of the CMPA in Fig. 1 are illustrated in Fig. 2(a) and Fig. 2(b) for an activated pixel i. In this pixel, either M2 or M3 is opened and provides current to the input regulated current mirror composed of opamp A, M0, and M6, in Fig. 2(b), or opamp A, M1, and M7, in Fig. 2

Table 2　Specifications from the preliminary experimentations

Typical assembly voltage	1.5 ～2.5V
Min. assembly voltage	1V
Optimized voltage duration	60s
Max. potential variation	<10mV
Assembly current range	～10nA to ～10μA
Max. signal bandwidth	<10kHz

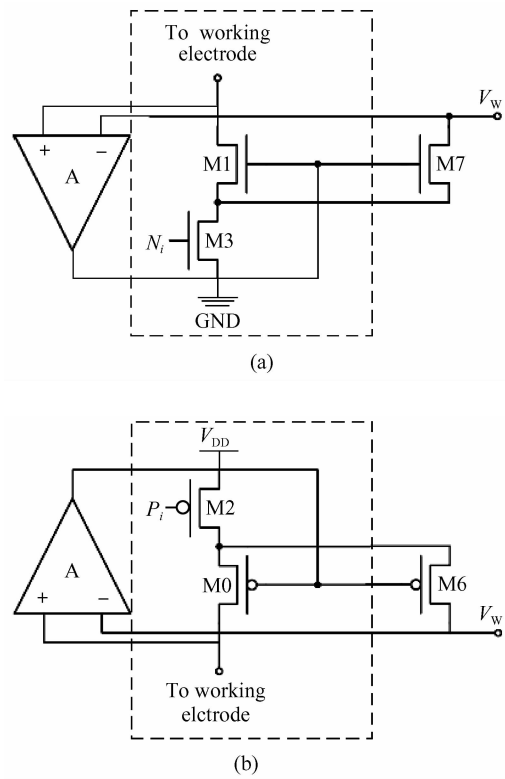

Fig. 2　Transistor level implementation of the proposed CMPA (a) N branch of proposed CMPA; (b) P branch of the proposed CMPA

(a), during the assembly process, which implies the positive or negative assembly voltage of $V_W - V_C$ or $-|V_W - V_C|$ on the activated working electrode with respect to the counter electrode, depending on the logic states of signals P_i and N_i in Table 1. The electrode potential is stabilized from the feedback mechanism introduced by opamp A. The DC gain of the CMPA (or equivalently $(W/L)_6/(W/L)_0$ and $(W/L)_7/(W/L)_1$) is designed to be 40dB (or 100dB). Moreover, the parts inside the dashed boxes are pixel circuits which are duplicative, while the parts outside, including opamp A, M6, and M7, are shared for all 16 pixels. For a specific address, only one copy of the pixel circuit is connected to the shared CMPA, which is controlled by logic signals P_i, N_i, SP_i, and SN_i after decoding, and switches S0, M4, and M5. This architecture simplifies the pixel circuitry, thus further shrinking the pixel area and reducing the hardware expenses and power consumption for the CMPA.

An opamp A with rail-to-rail input common-mode range and Class-AB output stage is also incorporated to serve for the feedback mechanism in the CMPA, which is depicted in Fig. 3. The opamp uses the complimentary folded-cascode input stage composed of transistors M0 to M13 to achieve the rail-to-rail input common-mode range, enable the required assembly voltage, and reduce the input-referred noise to sta-

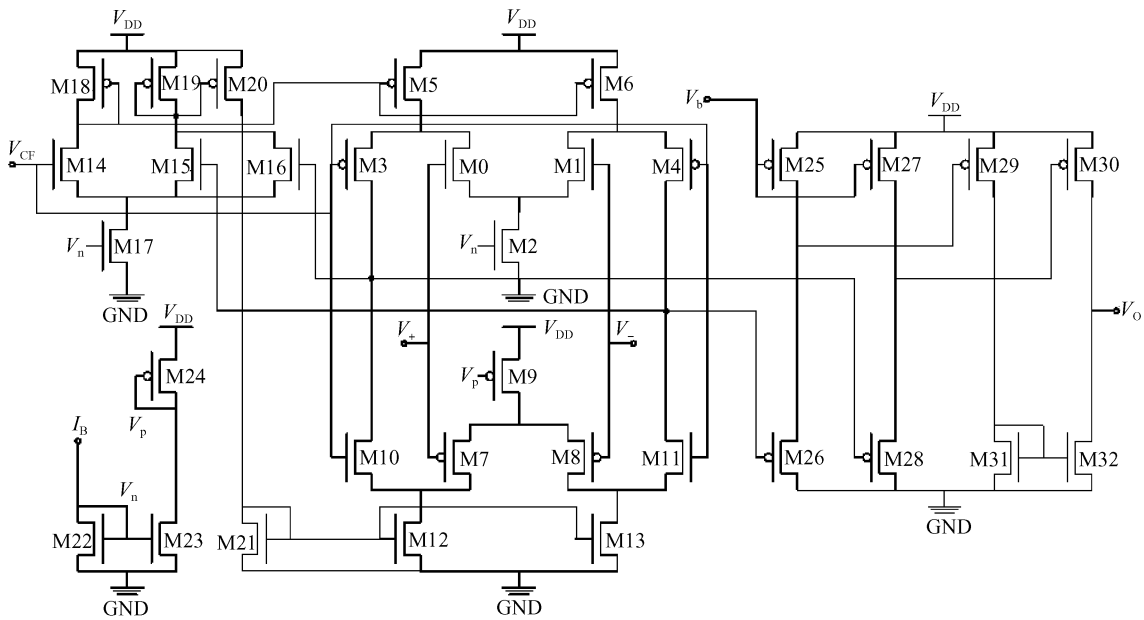

Fig. 3 Transistor level implementation of the proposed opamp with rail-to-rail input common-mode range and Class-AB output stage

bilize the potential. We incorporate the Class-AB output stage composed of transistors M29 to M32 to accommodate the dynamic range requirement in Table 2. Transistors M14 to M21 function as the common-mode feedback circuit and provide biasing voltage for the folded-cascode input stage. M25 to M28 form two source followers to match the DC voltage between stages, while the other biases are served by M22 to M24 from a current $I_B = 1\mu A$.

2.3 Potential variation and noise current

The potential variation on the working electrode is due to: (1) finite gain of the opamp, (2) input referred noise, and (3) the input referred offset of the opamp. If G^{DC} is the DC gain of the opamp, the potential variation, V_{ft}, due to (1) can be expressed as

$$V_{ft} = \frac{V_{max}}{G^{DC}} \tag{1}$$

An opamp with large G^{DC} (over 70dB in the design) is preferred to reduce the potential variation.

Transistors M0, M1, M3～M8, and M10～M13 in the first stage contribute to the overall noise. The noise current power spectral density, S_I, in a MOS transistor is given by[12,13]

$$S_I = 4\gamma kTg_m + \frac{K_F I_{ds}^{A_F}}{f^{E_F} C_{ox} WL} \tag{2}$$

where γ is the thermal noise parameter, g_m is the transconductance, I_{ds} is the drain-source current, C_{ox}, W, and L are the gate capacitance per unit area, transistor width, and length, respectively, and k, T, and f are the Boltzman constant, temperature, and frequency, respectively. K_F, A_F, and E_F are the flicker noise parameters with the typical values of 2×10^{-25}, 2, and 1, respectively. The corner frequency f_c, where thermal noise and flicker noise exhibit the same power density, is calculated as 5.4Hz using parameters provided by the foundry, which is much smaller than the unit gain bandwidth. Therefore, flicker noise is negligible in the proposed opamp, and the input referred noise voltage V_{irn} can be characterized by

$$\overline{V}_{irn}^2 = \frac{8\gamma kT(g_{m0} + g_{m3} + g_{m5} + g_{m7} + g_{m10} + g_{m12})}{(g_{m0} + g_{m7})^2} \tag{3}$$

where g_{mj} is the transconductance of transistor Mj, $j = 0, 1, \cdots, 32$. $\overline{V}_{irn}$ can be diminished by increasing the biasing currents and aspect ratios of the input differential pairs, but trades off with the power consumption and the physical area.

A Monte-Carlo simulation was performed to characterize the input referred offset using the mismatch parameters provided by the foundry. In the worst case of $V_{CM} = 0V$, the overall potential variation due to the above three issues is 5.88mV, which implies an 8bit of potential resolution and satisfies the condition in Table 2.

Table 3 Summary of performances of proposed CMPA

CMPA	N branch	P branch
DC gain/dB	40	40
Min. 3dB bandwidth/MHz	4.4	3.7
Assembly voltage range/V	−1.6～1.6	−1.6～1.6
Max. potential variation/mV	5.88	5.87
Potential resolution/bit	8	8
Max. noise current/pArms	135	118
Max. offset current/nA	7.1	7.1
Power supply/V	1.8	1.8

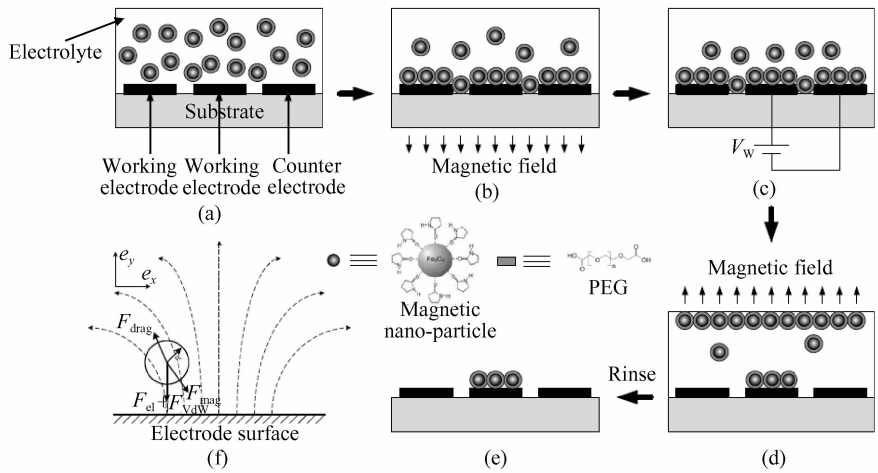

Fig. 4　(a)～(e) Flowchart of electromagnetically assisted assembly of MNPs based on the proposed IMA; (f) Force diagram of MNP within the electrolyte

The noise current of the CMPA is induced by: (1) input referred noise of opamp A, and (2) intrinsic noise from the current mirror transistors. According to Eq. (2), the second part decreases with the assembly current; while the reduction of the first part has been discussed above following Eq. (3). Simulation shows that issue (1) dominates the noise current over the specified current range of ～10nA to ～10μA in Table 2, especially for the small current cases. The circuit performances of the proposed CMPA are summarized in Table 3 and meet the specifications in Table 2.

3　Principles of MNP assembly

30nm PEG coated MNPs in an aqueous buffer with the concentration of 0.1% are used as a prototype to demonstrate the selective bio-assembly in the experiment. The PEG coated MNPs are synthesized through the thermal decomposition reaction of iron (III) acetylacetonate (Fe(acac)3) and the organic solvents of 2-pyrrolidinone together with α, ω-dicarboxyl-terminated PEG (HOOC-PEG-COOH), whose chemical structures are presented in Fig. 4. The detailed synthesis method and chemical properties are discussed in Refs. [8,9].

According to Refs. [14,15], nanometer scale ion oxide particles exhibit superparamagnetism, namely, they can be magnetized in a magnetic field and the magnetic susceptibility, χ, is much larger than 1. However, there is no magnetic memory. Once the external field is removed, the particles redisperse and behave like a non-magnetic material. The force on the superparamagnetic particle inside the magnetic field depends on the volume of the particle, V, the difference of magnetic susceptibilities between the magnetic particle and its surrounding buffer medium, $\Delta\chi$, and the strength and gradient of the applied magnetic field, B and ∇B,

$$F_{mag} = \frac{V\Delta\chi}{\mu_0}(B\nabla)B \tag{4}$$

where μ_0 is the magnetic permeability in vacuum[16].

Figure 4 shows the principles of the assembly of PEG coated MNPs. The force diagram of MNP within the electrolyte is shown in Fig. 4(f). In this system, five types of major forces are being applied on a MNP, magnetic force, F_{mag}, electrostatic force, F_{el}, Van der Waals force, F_{VdW}, random Brown fluctuation force due to the collision between MNP and water molecules, F_{Br}, and the hydrodynamic drag force, F_{drag}, which is caused by the friction within the fluid, and is smaller than the previous four forces in magnitude around the electrode surface. The other non-dominant forces, such as the buoyancy force etc., are omitted. Because of the random nature of Brown Motion, F_{Br} is not shown in Fig. 4(f).

First, a magnetic field is applied from the backside of the IMA chip to pre-concentrate the MNPs in the electrolyte onto the electrode area (Fig. 4(b)). But since the gradient of magnetic field, ∇B, around the electrode surface is relatively small compared to that within the electrolyte, according to Eq. (4), F_{mag} is small. Therefore, there are no close contacts between the MNPs and the electrode surface, and F_{VdW} is smaller than F_{Br}, so no assembly occurs. As a positive voltage V_W is applied on the working electrode with respect to the counter electrode, since these PEG coated MNPs are negatively charged within the electrolyte[8,9], they are further attracted by F_{el} onto the activated working electrode. Due to the close contact between the MNPs and surface of the activated electrode induced by F_{el}, F_{VdW} is much larger than F_{Br}. These MNPs are eventually immobilized on the elec-

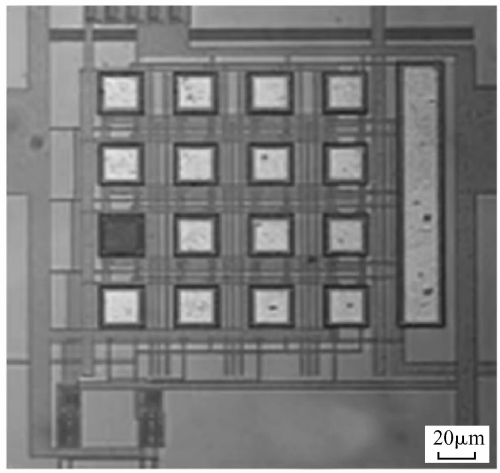

Fig. 5 Microscope picture of the 30nm MNPs assembly on electrode 〈0001〉 and the contrast experiment on electrode 〈0000〉 of the CMOS IMA

trode surface specifically due to the Van der Waals attraction (Fig. 4(c)). Subsequently, an opposite magnetic field is applied to remove the residual MNPs on the inactivated working electrode (Fig. 4(d)), and the whole chip is rinsed by DI water (Fig. 4(e)). The current induced by the assembly process is read out by the buried pixel CMOS circuit underneath the working electrode and further amplified by the shared current mode preamplifier (CMPA).

4 Experiment and discussion

The proposed IMA is designed in a SMIC 0.18μm standard CMOS mixed-signal process with a 1.8V power supply. In this process, the IMA bio-chip is fabricated on the p type Si wafer with a resistivity of 0.01$\Omega \cdot$ cm, and the electrode topology is shown in the die micrograph illustrated in Fig. 5. The selective assembly of 30nm negatively charged MNPs is validated by experiments in terms of atomic force microscopy (AFM) and scanning electron microscopy (SEM), which in turn verifies the correctness and feasibility of the proposed IMA.

4.1 Electrode fabrication

The Al electrodes on the IMA bio-chip can be fabricated from the post CMOS process after fabrication, which is intrinsically compatible with SMIC 0.18μm standard CMOS technology: (1) A mask with electrode patterns is aligned to the fabricated bio-chip; (2) A step of lithography/etching process is applied on the SiO_2/Si_3N_4 passivation layer to expose the Al electrodes of the chip; and (3) Before the experiments, the chip is further rinsed by the diluted acid to remove the thin oxide layer on the electrode. The fabricated 16 pixels of the 19μm$\times$19μm electrode array and the 140μm$\times$19μm counter electrode are illustrated in Fig. 5.

4.2 Preparation experiments and discussion

Before integration with the IMA chip, we also prepared experiments on the 150μm$\times$150μm separate electrodes to find suitable conditions for effective MNP assembly and the integration with our proposed IMA chip. According to the experiment, the assembly voltage V_A should be larger than a threshold of 1.2V to achieve effective assembly, while the thresholds of magnetic field B and time t appear around 0.5T and 10s, respectively. On the other hand, excessively large values of V_A, B, and t will substantially increase the clustering of MNPs on the electrode, which may limit the down-scaling of the electrode dimensions and degrade the resolution. The "sweet conditions" are optimized as $V_A = 1.6$V, $B = 1.2$T, and $t = 60$s.

According to the experimental result, MNPs are effectively assembled on the Al electrode surface for $1.2\text{V} < V_A < 2.0\text{V}$, while larger values of V_A will result in bubbles on the electrode surface due to the electrochemical oxidization of Al, thus destroying the assembly of MNP. Although Au or Pt electrodes can avoid the bubbling issues for $V_A > 2.0$V, MNP clustering issues may still come into the system since V_A is substantially larger than its optimized value of 1.6V in this case. Moreover, the post fabrication process for Au and Pt electrodes is much more complicated and less compatible with the standard CMOS process compared to Al electrodes[7]. Meanwhile, V_A should be nominally within $0 \sim 1.8$V due to the power rail limitation, and within this range Au or Pt shows no significant superiority over the Al electrode in the experiment.

Contrast experiments in Fig. 6 are also made on the separate electrodes to validate the assembly scheme illustrated in Fig. 4. Due to the absence of assembly voltage, MNPs can not be assembled on the electrode surface in Fig. 6(a). In this case, since F_{mag} is small close to the surface, there is no close contact between the MNPs and the electrode surface. F_{VdW} is smaller than F_{Br}, so no assembly occurs. In Fig. 6(b), the assembly voltage immobilizes some MNPs on the electrode surface, however, due to the absence of a magnetic field, MNP concentration is relatively small around the surface and the efficiency of assembly is low. By following Fig. 4, the MNPs efficiently assembly on the electrode surface, as is shown in Fig. 6(c), which in turn validates the electromagnetic MNP assembly scheme in Fig. 4.

4.3 Integration experiments and discussions

In the integration experiment, a +1.6V of opti-

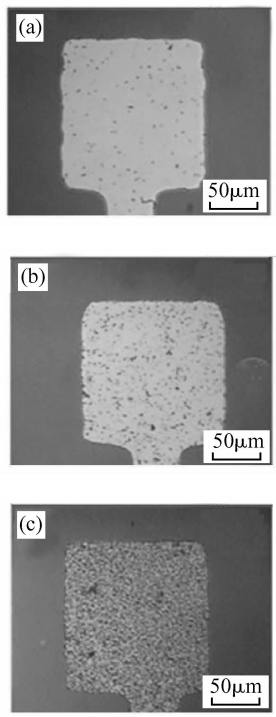

Fig. 6　Contrast experiments on the separate electrode to validate the principles of the electromagnetic assembly of MNPs (a) Result for $V_A = 0V$, $B = 1.2T$, and $t = 60s$; (b) Result for $V_A = 1.6V$, $B = 0T$, and $t = 60s$; (c) Result for $V_A = 1.6V$, $B = 1.2T$, and $t = 60s$

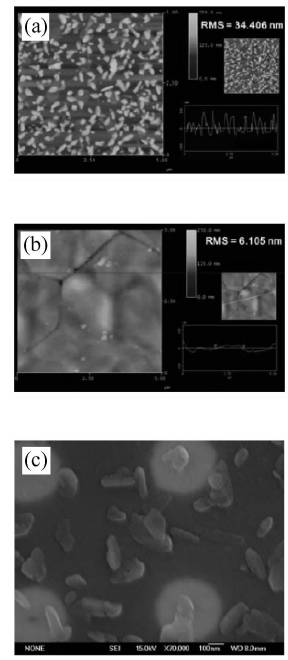

Fig. 7　(a) AFM picture of 〈0001〉 electrode surface after the assembly of 30nm MNPs　The area shown in this picture is 5μm ×5μm; (b) AFM picture of 〈0000〉 electrode surface without assembly of 30nm MNPs　The area shown in this picture is 5μm ×5μm. The intrinsic surface roughness on the working electrode is about 6.1nm; (c) SEM picture of 〈0001〉 electrode surface after the assembly of 30nm MNPs

mized assembly voltage of the activated working electrode is applied with respect to the counter electrode. According to the decoding scheme, the 16 electrodes in Fig. 5 are addressed as 〈0000〉, 〈0001〉, …, 〈1111〉 from the bottom-left to top-left vertically, and from the left column to the right column horizontally.

First, the 〈0000〉 electrode is activated for 60s without MNPs in the aqueous buffer. As is expected and shown in Fig. 5, no evidence is observed in the microscopy. Then electrode 〈0001〉 is activated for 60s in the aqueous buffer with PEG coated MNPs. After the rinsing process, the electrode surface becomes dark in Fig. 5. Consequently, we conclude from the contrast experiment above that the PEG coated MNPs are evidently assembled on electrode 〈0001〉 by the IMA. The AFM images of the contrast experiment above in Figs. 7(a) and 7(b) show the surface morphology of electrode 〈0001〉 and 〈0000〉, which gives direct evidence of the assembled 30nm MNPs. Furthermore, the closer view provided by the SEM image shown in Fig. 7(c) indicates that some of the assembled MNPs are gathered into clusters of a few particles and become larger in dimension, which limits the down-scaling of the electrode dimensions and makes the fabrication of a sub-100nm biosensor and integration with the CMOS process challenging in the future. The above experiment was successfully repeated on different electrodes and multiple chips, which verified the repeatability and robustness of the integration experiment.

In the experiment, the measured potential variations due to the input referred offset and noise are 3.5mV and 15μVrms, respectively, and the current noise is around 25.3pArms. The other parameters are summarized in Table 4 and satisfy the specifications in Table 2. Meanwhile, the measured parameters are consistent with the post simulation result in Table 3, but better than the worst case estimations made in the simulation.

Moreover, the bio-assembly current on working electrode 〈0001〉 during the above process is measured and amplified by the *P* branch of CMPA in the pro-

Table 4　Summary of measured parameters from the proposed IMA

DC gain	39.8dB
Overall potential variation	3.52mV
Potential resolution	8bit
Bio-assembly voltage	1.6V
Max. bio-assembly current	2.7μA
Saturated bio-assembly current	63nA
Max. noise current	25.3pArms
Max. offset current	5.9nA
Power supply	1.8V

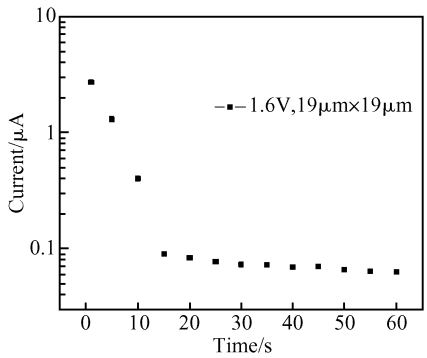

Fig. 8 MNP assembly current as a function of the duration of assembly voltage The solid squares represent the measured assembly currents

posed IMA, and the results are shown in Fig. 8. The assembly current decreases monotonously from 2.7 to 0.1μA within 15s from the start point, and gradually saturates to ~ 70nA at the end of the assembly process. This is because after the assembly voltage is applied on the activated working electrode with respect to the counter electrode, the MNPs in the aqueous buffer experience a large electric field, move toward the electrode, and are eventually immobilized on the electrode surface. However, as time elapses, the previously assembled MNPs, which are negatively charged, shield the applied electric field, and in turn reduce the effective electric field being applied on the following MNPs in the buffer. Thus, the assembly current decreases. Moreover, due to the reduction of assembly current, the decreasing speed of the effective electric field on MNPs becomes smaller as a function of time, which accounts for the saturation of the bioassembly current in Fig. 8. The measured current again shows that the MNP assembly is mainly due to the existence of an electric field or assembly voltage on the selected working electrode, while the magnetic field pre-concentrates the MNPs around the electrode surface and enhances the efficiency of the following assembly process.

5 Conclusion

In this paper, a CMOS IMA targeting an electromagnetic selective assembly of charged MNPs is proposed and designed in a SMIC 0.18μm CMOS mixed signal process. The circuit integrates the 16 pixels of a 19μm×19μm electrode array, a 140μm×19μm counter electrode, a CMPA, adigital decoding circuit, and control logics on a single chip. It is capable of providing a −1.6~1.6V assembly voltage, a potential resolution of 8bit, and a current gain up to 39.8dB, biased at a current of 1μA, while the offset and noise are smaller than 5.9nA and 25.3pArms, respectively. Experimental results show that the proposed IMA satisfies the prerequisite specifications and that it is feasible to selectively assemble the prototype of 30nm PEG coated MNPs on the activated working electrode by the applied voltage. In fact, the PEG coated MNP can be further conjugated with multiple bio-species (DNA molecules, proteins, or antibodies) on the surface and selectively assembled on the activated working electrode from the proposed approach, which may significantly improve bio-sensing efficiency, specificity, and diversity of IBS.

References

[1] Drummond T G, Hill M G, Barton J K. Electrochemical DNA sensors. Nature Biotechnology, 2003, 21(10): 1192

[2] Li Z, Chen Y, Li X, et al. Sequence-specific label-free DNA sensors based on silicon nanowires. Nano Lett, 2004, 4(2): 245

[3] Guiducci C, Stagni C, Zuccheri G, et al. A biosensor for direct detection of DNA sequences based on capacitance measurements. Proc of ESSDERC, 2002: 479

[4] Xu C, Li J, Wang Y, et al. A CMOS-compatible DNA microarray using optical detection together with a highly sensitive nanometallic particle protocol. IEEE Electron Devices Lett, 2005, 26(4): 240

[5] Han S, Yu H, Murmann B, et al. A high-density magnetoresistive biosensor array with drift-compensation mechanism. ISSCC Dig of Tech Papers, 2007: 168

[6] Augustyniak M, Paulus C, Brederlow R, et al. A 24×16 CMOS-based chronocoulometric DNA microarray. ISSCC Dig of Tech Papers, 2006: 59

[7] Thewes R, Paulus C, Schienle M, et al. A CMOS medium density DNA microarray with electronic readout. Mater Res Soc Symp Proc, 2005, 869: D3.4.1

[8] Li Z, Wei L, Gao M Y, et al. One-pot reaction to synthesize biocompatible magnetite nanoparticle. Adv Mater, 2005, 17: 1001

[9] Li Z, Chen H, Bao H, et al. One-pot reaction to synthesize water-soluble magnetite nanocrystals. Chem Mater, 2004, 16(8): 1391

[10] Zhang L, He X, Yu Z. Design and implementation of ultra low current sensing amplifier with pico-ampere sensitivity aiming at bio-sensor applications. Chinese Journal of Electronics, 2007, 2: 247

[11] Zhang L, Yu Z, He X. A statistical method in characterizing CMOS process fluctuations in subthreshold current mirrors. Journal of Semiconductors, 2008, 29(1): 82

[12] Tsividis Y P. Operation and modeling of the MOS transistor. New York: McGraw-Hill, 1988

[13] Sarpeshkar R, Delbruck T, Mead C A. White noise in MOS transistors and resistors. IEEE Circs Dev Mag, 1993, 9(6): 23

[14] Bean C P, Livingstone J D. Superparamagnetism. J Appl Phys, 1959, 30: 120

[15] Lefebure S, Dubois E, Cabuil V, et al. Monodisperse magnetic nanoparticles: preparation and dispersion in water and oils. J Mater Res, 1998, 13: 2975

[16] Wirix-Speetjens R, Fyen W, Xu K, et al. A force study of on-chip magnetic particle transport based on tapered conductors. IEEE Trans Magnetics, 2005, 41(10): 4128

一种具有片上译码/放大功能的微阵列电路及其与生物纳米系统的集成*

张　雷[1,†]　顾　臻[2]　余志平[1]　贺祥庆[1]　陈　涌[2]

（1 清华大学微电子学研究所，北京　100084）
（2 加州大学洛杉矶分校机械与航天工程系，洛杉矶　90095，美国）

摘要：提出了一种用 SMIC 0.18μm CMOS 混合信号工艺实现的全集成 CMOS 微阵列生物芯片，并成功地实现了其与一种新的生物纳米系统的集成.该电路实现了 19μm×19μm 电极的 4×4(16 单元)阵列，反相电极，电流模式放大器，译码电路，以及逻辑控制电路的单片集成，并能够提供 -1.6～1.6V 的组装电压，8bit 的电位分辨率及 39.8dB 的电流增益，电源电压为 1.8V，而失调和噪声电流分别为 5.9nA 和 25.3pArms.在实验中，利用该电路实现了对 30nm 聚乙烯醇包裹的磁性粒子的片上选择性组装，并对实验结果进行了讨论，从而验证了该电路的正确性和该集成方法的可行性.

关键词：CMOS 生物芯片；集成 CMOS 微阵列电路；全集成；电路模式放大器；选择性组装；磁性纳米粒子
EEACC：1205；1280；3120
中图分类号：TN432　　**文献标识码**：A　　**文章编号**：0253-4177(2008)10-1947-09

* 国家自然科学基金(批准号：60236020，90307016)，Intel 基金，SMIC 大学计划项目及美国加州 Dan Yang 博士私人基金资助项目
† 通信作者.Email：zl99@mails.tsinghua.edu.cn
2008-04-06 收到，2008-06-03 定稿